Ethiopian Journal of Natural and computational Science(EJNCS)

Ethiop J Nat Comp Sci 2026, Volume 6, Issue 1

Original Research Article

Chemical Characterization and Antibacterial Properties of Anthraquinones from *Senna didymobotrya*

Patrick Amani Katana*, Regina Kemunto Mayaka, and Josiah Ouma Omolo

Faculty of Science, Department of Chemistry, Egerton University, 536-20115 Njoro-Kenya

*Corresponding author: email: patrickamani544@gmail.com

Patrick A. Katana: 0009-0008-7830-9610

Article History:

Received: June 20, 2025

Accepted: December 11, 2025

Published: January 19, 2026

Print ISSN 2710-0200

Electronic ISSN 2710-0219

ABSTRACT

Bacterial infections remain a critical global health challenge intensified by the rising bacterial resistance to conventional medicines. This study evaluated the antibacterial activity of anthraquinones from *Senna didymobotrya*. Thin layer chromatography-direct bioautography (TLC-DB), chromatographic separations, and spectroscopic techniques proved vital research methods. The crude extracts from the plant were screened through TLC-DB method which revealed terpenoids, alkaloids, flavonoids, and phenolics. Three anthraquinones were isolated, identified, and verified by UV-Visible spectrophotometer and Nuclear Magnetic Resonance, and ESI-MS Spectrometry methods. TLC-DB bioassay method showed noTable inhibition of Pseudomonas aeruginosa of up to 13±0.00 mm for seedpod extracts and Staphylococcus aureus of 11±0.00 mm to 13±0.00 mm across samples from leaf, stem bark, and seedpod extract. Escherichia coli and Salmonella typhimurium were not inhibited. Among the isolated compounds, 1, 8-dihydroxy-3-methoxy-6-methylanthracene-9, 10-dione and 1, 8-dihydroxy-3-methylanthracene-9, 10-dione produced zones of 11±0.10 mm and 12±0.15 mm, respectively, while 1, 5-dihydroxy-3-methylanthracene-9, 10-dione showed weaker activity of 9±0.12 mm against P. aeruginosa. Due to the observed anthraquinone antibacterial activity, it is recommended for use in phytotherapy, particularly in formulations aimed at treating various ailments, including tumour cancer. These findings scientifically validated the traditional use of *S. didymobotrya* and highlighted the anthraquinones as promising leads against antibiotic-resistant pathogens deserving further pharmacological assessments.

Keywords: Antibacterial, anthraquinones, bacterial-resistance, phytochemicals, *Senna didymobotrya* , TLC-DB bioassay.

INTRODUCTION

The *S. didymobotrya* plant (Family; *Fabaceae*), is commonly known as popcorn senna or peanut butter cassia. It is a multi-stemmed shrub or small tree native to tropical East and Central Africa. It grows 0.5 to 5 m tall, although it can reach up to 9 meters under preferred conditions. It

mostly found along roadsides, in Savannah land, and evergreen bush lands (Diab et al., Senna. 2024).

The plant is characterized by pinnately compound leaves with 8-18 pairs of oval leaflets, bright yellow flowers, and flat, brown seed pods. Its foliage emits a characteristic odour resembling that of buttered popcorn or crushed peanut butter. *Senna didymobotrya* prefers full sun and well drained, moist soil, tolerates light frost, and is grown globally in tropical and subtropical regions for both ornamental and traditional medicinal purposes (Khadhum et al., 2025).

Traditional medicinal plants are continuously being studied for their medicinal value with traditional healers remaining the hope for treating ailments in the rural settlements. *Senna didymobotrya* decoctions from the leaves, roots, and stems are used to treat abdominal pain, constipation, dysentery, diarrhoea, malaria, fever, jaundice and expelling intestinal worms (Osunga et al., 2023). It is also applied on top of the skin to cure skin disease like ringworm and fungal infections. Its traditional medicinal use are supported by the vast phytochemicals present in *S. didymobotrya* including anthraquinones, flavonoids, alkaloids, and phenols (Sadia et al., 2022). *Senna didymobotrya* is distinguished for its invasive characteristics and ecological impacts but has gained attention for its secondary metabolites of the anthracene origin with potential therapeutic effects (Weldemariam et al., 2021; Alemayehu et al., 2015).

Anthraquinones are naturally occurring aromatic compounds found in various plants of the genus Senna, where they primarily exist as glycosides. These compounds possess a characteristic anthracene structure with two ketone groups (Murdani et al., 2024). The compounds are well known for their potent stimulant laxative effects. Anthraquinones antibacterial potency varies with chemical structure where increased polarity and certain substituents like hydroxyl groups enhance membrane disruption, while others like methoxy groups may reduce activity (Qun et al., 2023). The anthraquinone compounds combat bacterial infections through several mechanisms. The mechanisms include disruption of bacterial cell wall and membrane causing leakage of vital intracellular component, impairing nutrient uptake and waste excretion by the bacteria.

Anthraquinones also inhibit biofilm formation thereby reducing bacterial protection and enhance vulnerability to treatments. They also block bacterial endotoxins lessening virulence, inhibiting nucleic acid and protein synthesis thereby stopping bacterial growth (Raghuveer et al., 2023; Havelikar et al., 2025). Anthraquinones and their derivatives however, can be optimized and modified structurally to improve their efficacy especially in the context of curbing and addressing the rising cases of antimicrobial resistance (AMR) (Saleem et al., 2011; Odonkor, 2011; Addo, 2018). These properties are ideal since the plant is used in traditional and modern medicine to treat constipation and prepare patients for bowel procedures. Anthraquinones also exhibit anticancer properties however, their use require caution due to possible side effects with prolonged consumption (Olofinsan et al., 2025).

The early 21st century has seen a rapid rise in antibiotic resistance. A crisis attributed to various correlated factors, including the misuse and overuse of antibiotics, genetic mutations in bacterial strains, inadequate hygiene practices, and a general lack of awareness about bacterial infections and their resistance mechanisms (Saleem et al., 2011; Odonkor, 2011; K.K. Addo, 2018). Historical trends indicate that resistance emerged shortly after the introduction of antibiotics. For instance, resistance to sulphonamides and penicillin was observed in the late 1930s, with subsequent resistance against tetracycline and chloramphenicol by the 1950s (Aminov, 2017). The emergence of methicillin-resistant Staphylococcus aureus (MRSA) followed shortly after

methicillin's introduction in 1959, and more recently, resistance to daptomycin and linezolid was reported within five years of their release (Li and Webster, 2018).

The effects of antibiotic resistance are severe. It contributes to increased morbidity and mortality rates and imposing significant economic burdens on healthcare systems (WHO, 2021). According to the World Health Organisation (WHO), nearly 5 million deaths occur annually and are caused by drug-resistant bacterial infections. Moreover, the GLASS 2025 WHO report indicated further that one in six bacterial infections resist common antibiotics. E.coli and K. pneumonia strains show 40-55 % resistance to key treatments. WHO also warns that, without better stewardship by 2035, projections warn of doubled resistance to the last resort antibiotics as there is no major news on development of novel classes of effective antibiotics (WHO, 2021). In response to this pressing issue, researchers are investigating innovative strategies such as bacteriophage therapy, which employs viruses that specifically target bacteria (Viertel et al., 2014; Kortright et al., 2019). However, despite early successes in bacteriophage therapy, challenges remain due to the specificity of phage and their rapid clearance from hosts (Organization, 2021; Pulingam et al., 2022; Laxminarayan et al., 2020).

The objective of this research was to isolate secondary metabolites with antibacterial properties from *S. didymobotrya* . This was made possible by employing bioassay-guided fractionation method utilizing thin layer chromatography-direct bio autography (TLC-DB).

MATERIALS AND METHODS

In February 2023, plant materials of *S. didymobotrya* (leaves, stem bark, seedpods) were collected from the Egerton University Botanic Garden in Njoro, Kenya. After air-drying to a constant weight, they were ground and stored in the chemistry laboratory for further use.

Crude extraction

The ground material of the stembark, seedpods, and leaves of *S. didymobotrya* were weighed to get the total mass of the powder then extracted separately using the chosen solvents. Clean, 2 L conical flasks were filled with the ground plant materials and soaked at room temperature for three days by cold-extraction with DCM (14 litres), methanol (9 litres), and acetone (18 litres). The extraction process was repeated thrice for each solvent to ensure maximum extraction. There was timely agitation and shaking of the contents to ensure all material were homogeneously soaked and extracted. The extracts were filtered through Whatman No. 1 filter paper. Each filtrate was concentrated in a rotary evaporator at reduced pressure and temperature (40-50 °C) until dry. The crude extracts were weighed and stored for future use in sterile, sealed containers at 4 °C (Latolla et al., 2023).

Qualitative determination of the chemical constituents

The phytochemical analysis of *S. didymobotrya* was performed using direct bioautographic analysis to identify the phytoconstituents of the plant. The qualitative tests for preliminary phytochemical follow the aforementioned standard method utilized for the qualitative phytochemical (Nyamwamu et al., 2015; Shaikh and Patil, 2020).

Thin layer chromatography-direct bioautographic method

The Thin Layer Chromatography - Direct Bioautography (TLC-DB) method was employed for the initial phytochemical screening of *S. didymobotrya* rude extracts to identify alkaloids, phenols,

flavonoids, and triterpenes. Pre-coated TLC plates (DC-Fertigplatten SIL G-25, Macherey-Nagel, Germany) were used with a DCM-hexane (70:30) solvent system for improved compound separation. Visualization was conducted under white light and UV light (Uvitec, 365 and 254 nm). Various spray reagents were developed to help identify and separate the compounds of interest from other substances. For example, Tin (IV) chloride was used for polyphenols, while Dragendorff's reagent identified alkaloids, and Antimony (III) chloride was used for flavonoids (Latolla et al., 2023).

Dragendorff's reagent was prepared for the detection of the presence of alkaloids. The reagent was prepared by taking 0.85 g of bismuth nitrate pentahydrate then dissolved in 40 mL of distilled water and 10 mL of glacial acetic acid, followed by the addition of 10 mL of 80% potassium iodide solution. The working spray was made by mixing 12.5 mL of this stock solution with 87.5 mL of water and 25 mL of glacial acetic acid. Yellow, orange, and red bands on the TLC plate indicated the presence of alkaloids after development and drying at 105 °C (Febrina et al., ,2025).

Iron (III) chloride reagent was prepared for the qualitative test of phenolic compounds. Iron (III) chloride was prepared by measuring100 mL of 0.5 M hydrochloric acid and 5 mL of methanol and mixed with iron (III) chloride hexahydrate. After spotting and incubating the thin layer chromatography plates with crude extracts, the spray reagent was applied, dried at 105 °C, and the appearance of greenish bands confirmed the presence of phenolic compounds (Athipornchai, and Klangmane, 2021).

The presence of flavonoids was ascertained by utilising antimony (III) chloride reagent. About 10 g of Antimony (III) chloride was dissolved in 100 mL of chloroform to make a 10% solution. After treating the already developed TLC plates with this reagent and heating at 105 °C for five minutes, the plates were examined under UV light at 365 nm. The presence of bluish bands indicated the detection of flavonoids (Afrokh et al, 2023).

Tin (IV) chloride pentahydrate spray reagent was used for the detection of triterpenes, phenols, steroids, and polyphenols. The tin (IV) chloride pentahydrate spray reagent was made by combining 10 mL of the standard tin (IV) chloride solution with 160 mL of an aqueous mixture of glacial acetic acid and chloroform (5:5). The TLC plates were treated with the prepared reagent, then heated at 105 °C for 5 minutes, and observed under visible and long wavelength UV light (Ranaweera et al., 2024).

The test for phenols, terpenoids and steroids presence was further done using the p-anisaldehyde-sulfuric acid spray reagent. To prepare the p-anisaldehyde-sulfuric acid spray reagent for terpenoids and phenolic compounds, 1.0 mL of p-anisaldehyde was combined with 100 mL of glacial acetic acid and 2 mL of 97% sulfuric acid in a fume hood. The TLC plates were treated with this reagent, heated to 105 °C, and examined for green bands for phenolic compounds and violet bands for the presence of terpenoids and steroids (Latolla et al., 2023; Ranaweera et al., 2024).

UV-Vis spectrophotometric quantitative estimation of phytochemical content

The quantification of phytochemical content in crude *S. didymobotrya* extracts was done using UV-Vis spectrophotometric analysis.

Alkaloidal content

The alkaloid content was determined by dissolving 10 mg of the crude plant extract in 10 mL of 2 N hydrochloric acid (HCl). One millilitre of this solution was filtered into a separating funnel

and then washed three times with 10 mL of chloroform (CHCl3). The pH of the solution was neutralized with 0.1 M sodium hydroxide (Kobian Kenya Limited), followed by the addition of 5 mL of bromocresol green solution and 5 mL of phosphate buffer (pH 4.7). After thoroughly shaking the mixture, the alkaloid complex was extracted using 1, 2, 3, 4, and 5 mL of CHCl3. The extract was then diluted to the appropriate volume in a 10 mL volumetric flask (Abasum et al., 2016).

Preparation of reagents for alkaloids quantification

Bromocresol green solution was prepared by adding 69.8 mg of bromocresol green in a volumetric flask (Kobian Kenya Limited) then heated with 3 mL of 2 N sodium hydroxide (NaOH) and 5 mL of distilled water until fully dissolved. A 2 M phosphate buffer solution (pH 4.7) was prepared by adding 71.6 g of sodium phosphate (Kobian Kenya Limited) and adjusting the pH with 0.2 M citric acid. A citric acid solution was prepared by dissolving 42.02 g of citric acid (Kobian Kenya Limited) in 1 L of distilled water.

Preparation of standard curve for atropine alkaloid

The preparation of an atropine standard solution for alkaloid determination involved dissolving 10 mg of pure atropine (CAS No. 5908-99-6, Sigma Aldrich, USA) in 10 mL of distilled water to create a primary stock solution with a concentration of 100 µg/mL (100 ppm). For the calibration curve, aliquots of the stock solution (0.4 mL, 0.6 mL, 0.8 mL, 1.0 mL, and 1.2 mL) were transferred to separatory funnels, mixed with 5 mL of pH 4.7 phosphate buffer and 5 mL of bromocresol green (BCG) indicator, and extracted with chloroform to form a yellow complex. The absorbance of the chloroform layer was measured at 470 nm and a linear calibration curve was plotted using the prepared atropine aliquots concentrations. The quantification of the total alkaloids in the plant extracts were then correlated by the standard curve and the sample absorbance (Abasumet al., 2016).

Total phenolic content

The quantification of phenolic content in the plant extracts using the Folin-Ciocalteu (FC) method involved a redox reaction where phenolic compounds reduced the FC reagent (a phosphomolybdic-phosphotungistic acid complex), producing a blue chromophore that was measured spectrophotochemically. A standard calibration curve was prepared using gallic acid and the absorbance measured at 760 nm. For the sample analysis, a 0.2 mL aliquot of the plant extract was mixed with 2.5 mL FC reagent (HC12623401, Merck, Germany) and allowed to react for about 5 minutes before addition of 2 mL of 7.5 % w/v sodium carbonate to make the solution alkaline. After incubation for 30 minutes at 40 oC, the absorbance of the solution was measured using a UV-Vis K9000 spectrophotometer and the total phenolic content calculated using the calibration curve and was expressed as gallic acid equivalents (GAE mg/g) of the sample (Sánchez-Rangel et al., 2013).

Preparation of Folin-Ciocalteu standard solution

Folin-Ciocalteu standard curve for phenolic quantification was prepared by first preparing a 1 g/L gallic acid stock solution (Gallic acid monohydrate, CAS No. 5995-86-8, Sigma-Aldrich, USA). The stock solution was serial diluted to obtain a range of standard concentrations of 0.2, 0.4, 0.6, 0.8 and 1.0 g/L. for each concentration, a 0.2 mL aliquot was pipetted into a test tube, then 2.5 mL of the FC solution added. The mixture was incubated for 5 minutes then 2.5 mL of 7.5% w/v

sodium carbonate was added to initiate the colour reaction. The mixture was incubated for 30 minutes at 40 ^{0}C until a blue colour appeared then the absorbance read at 760 nm using a UV-Vis K9000 spectrophotometer. A plot of the absorbance values versus the gallic acid concentrations was generated to give a calibration curve that was used to quantify the total phenolic content in the plant extracts.

Total terpenes/terpenoids content

Ten milliliters of MeOH were used to dissolve 1 g of the crude extract. After filtering, around 5 mL was put into a test tube, combined with 2 mL of CHCl3 and 3 mL of pure sulfuric acid (H2SO4), and left to sit in an ice bath for 15 minutes. After that, the combination was allowed to sit at room temperature for two hours in the dark. The reddish-brown precipitate was decanted together with the supernatant. The precipitates were dissolved by adding 1.5 mL of MeOH and shaking until all of the material dissolved. Using a UV-Vis spectrophotometer (UV-Vis K9000), the total terpene concentration was determined at 538 nm (Aryal et al., 2018).

Linalool standard curve

A linalool calibration curve for quantifying the total terpenoids was prepared by dissolving 0.2 mg of pure linalool (Pcode 102524372, Sigma Aldrich, USA) in methanol to make a stock solution of 1000 ppm. A series of standard solutions with varying concentrations was made having 10, 8, 6, 4, 2, and 1 ppm by serial dilution using calibrated volumetric flasks. The absorbance of each standard was measured using a UV-Vis spectrophotometer (UV-Vis K9000). The absorbance of the standards was used to make a calibration curve against the linalool standard concentrations. The calibration curve was used to determine the terpenoid content in plant extracts by comparing their measured absorbance to the standard curve. The concentration of were measured at 538 nm and each analysis was performed in triplicate (Pedersen et al., 2003).

Laboratory strains of bacteria used as test organisms

The pathogenic organisms used in this study were sourced from the Egerton University Biotechnology Laboratory (from KEMRI-Kisumu) and included gram-negative Salmonella typhimurium (ATCC-14028), Escherichia coli (ATCC-25922), Pseudomonas aeruginosa (ATCC-12903), and gram-positive Staphylococcus aureus (ATCC-25923).

Bio-autographic screening of bioactive compounds

Media and sample preparation

Fresh cultures were obtained by growing the test strains overnight at 37oC for 24 hours. Mueller Hinton Agar was used for bacteria bioassay. Mueller Hinton Agar was prepared by dissolving 19 g in 500 ml of distilled water warmed to dissolve then sterilized by autoclaving at 121 oC for 15 minutes. About 20 mL of the autoclaved media was dispensed onto the pre-sterilized Petri dishes to cover about 4 mm of the petri dish depth. They were then covered and allowed to cool and harden at room temperature (Korir, 2012; wargiary et al., 2020).

Thin layer chromatography-direct bioautography bioassay

Bioactivity was assessed through the direct bioautographic examination. The plant materials were extracted using acetone, DCM, and methanol then concentrated to obtain crude extracts, the crude extracts were subjected to column chromatography and further column purifications to

obtain pure fractions. The crude extracts and the pure fractions (500 mg/mL) were dissolved in small volumes of methanol. A fresh overnight culture of test bacterium for Salmonella typhimurium, Pseudomonas aeruginosa, Escherichia coli, and Staphylococcus aureus were grown and adjusted to turbidity of 0.5 McFarland, then diluted to 1x106 CFU/mL in the Mueller Hinton Agar broth (M173-500G). TLC plates (Silica gel F254 aluminium) were pre-activated by heating at around 105 to 110 oC for an approximate of 15 to 20 minutes then cooled in a desiccator. The extracts were then applied as spots on the TLC plates using capillary tube. Development of the spot followed in a pre-saturated chamber using a mobile phase of 7:3 DCM:Hexane. After the appropriate height were reached by the solvent front, the TLC were removed and dried to remove any residual solvents (Amutha and Garapati, 2025; Bunya, and Lihan, 2025).

The dried TLC plates were then dipped into the bacterial suspension and covered the adsorbent layer of TLC. Incubation of the contents followed at 28-37 oC for 18 hours. Clear, colourless zones against a uniformly stained background indicated regions where the antibacterial compounds were located, directly linking activity to specific TLC bands. The inhibition zones were measured in mm then correlated to Rf values for the subsequent elution's and structural identification of active secondary metabolites. The solvent blanks showed no zones of inhibitions which indicated that the inhibition were due to the plant constituents (Choma and Jesionek, 2015; Šegan et al., 2021). For reproducibility purposes, the tests were done in triplicates.

Isolation of the bioactive compounds

Fractional isolation of acetone extract of *Senna didymobotrya*

The appropriate solvent system was determined by subjecting the acetone crude extracts to TLC elution using various solvent systems. Hexane: dichloromethane (3:7) was identified as the optimal solvent system and used as a model for column chromatography. A glass column with a diameter of 65 cm was packed with silica gel 60 (230–400 mesh, ASTM, Merck, Germany). The acetone crude extract was carefully combined with some amount of silica gel 60 (230-400 mesh, ASTM, Merck, Germany) to obtain a uniform mixture. The dried mixture was then gently loaded onto the packed column, followed by a small layer of acid-washed medium-fine sand obtained from May and Baker in Essex, England.

Elution was performed using a series of solvent systems, starting with 100% DCM (600 mL), followed by 70% DCM (400 mL), 35% DCM (400 mL), 15% DCM (400 mL), and finally 100% DCM (400 mL). The remaining contents in the column were then washed using 20% MeOH in DCM (400 mL). A total of 156 fractions, each containing approximately 25 millilitres, were collected and left to dry. Further TLC analysis and comparison of the fractions led to the pooling of those with similar components, resulting in a total of twenty-seven sub fractions. Further column chromatography was done to get more refined pure fractions. Fraction 2 (Act-02, 3.9 mg) and fraction 3 (Act-03, 3.7 mg) were crystalized with MeOH and analysed further by Electrospray Ionisation-Mass Spectroscopy (ESI-MS) and Nuclear Magnetic Resonance (NMR) yielding compounds 1,8-dihydroxy-3-methoxy-6-methylanthracene-9,10-dione and compound 1, 8-dihydroxy-3-methylanthracene-9,10-dione respectively due to their good masses.

Fractionation of dichloromethane extracts of *Senna didymobotrya*

Similarly, a uniform mixture of silica and the dichloromethane extract was finely ground with silica 60 (0.04-0.063 mm, ASTM, Merck, Germany). A total of 350 g of silica gel 60 (230–400 mesh,

ASTM, Merck, Germany) was then mixed with the least polar solvent to obtain a slurry that was then packed into a column (4.5–5.0 cm in diameter and 65 cm in length) using the slurry packing method (wet method). The prepared mixture was loaded onto the column and eluted with a series of solvent systems, beginning with 400 mL of 100% hexane, followed by 400 mL of a progressively polar solvent system up to 100% DCM. Subsequently, a 2:8 (MeOH: DCM) solution (400 mL) was passed through the column to extract any remaining sample material.

Twenty-nine fractions, each containing 20 mL, were collected and concentrated. Fractions exhibiting similar retention factors (Rf) were pooled and combined. The spots were analysed using a TLC ultraviolet lamp at wavelengths of 365 nm and 254 nm. Further refined column chromatography and purification of the pooled fraction yielded 3.9 mg of the compound 1,5-dihydroxy-3-methylanthracene-9,10-dione that was isolated and characterized using Nuclear Magnetic Resonance analysis.

Nuclear magnetic resonance analysis

The ^{1}H and ^{13}C-NMR data were recorded using a Bruker DPX-400 NMR spectrophotometer. The solvents used for recording the spectra were acetone and deuterated chloroform (CDCl3) and the chemical shifts (δ) expressed in parts per million (ppm).

Deuterated chloroform showed a relative peak at around δ 78-75 ppm in ^{13}C NMR and δ 7.26 ppm in the proton spectra. Acetone, however, showed an intense peak at δ 206.10 ppm for the ^{13}C NMR and a quintet at δ 2.05 ppm for the ^{1}H NMR spectra (400 MHz). The ^{1}H-NMR spectra appeared in its typical range of 0–14 ppm. Proton NMR peaks appeared as singlets (s), multiplets (m), triplets (t), doublets (d), and doublet of doublets (dd) reflecting coupling effects. The number of scans varied depending on suitability. The solvents peaks were excluded during compound structure elucidation. The ^{13}C NMR was ran at 298-300 K with a spectrometer frequency range of 75 to 400 MHz with varying number of scans.

The Distortionless Enhancement by Polarization Transfer (DEPT), Heteronuclear Single Quantum Coherence (HSQC), and Heteronuclear Multiple Bond Correlation (HMBC) spectra were ran at the same temperature as that of ^{13}C while varying the operating frequencies and number of scans and the information obtained were used to further determine the connectivity of the atoms in the molecule (Girardeau, 2023).

RESULTS

The results section outline the outcomes and observations made on all the tests conducted. The phytochemical profiling through TLC-DB method, quantification results, bioassays and structural elucidation follows this section.

Phytochemicals test results using bio-autographic method

Phenolic compounds were found to be generally present across all analysed samples. The phenolic and polyphenolic compounds overshadowed other phytochemicals in all parts of the plant as displayed in Figure 1 below. After treatment and spraying with derivatization reagents, the Dragendorff's reagent revealed yellow to orange bands to explain the presence of alkaloids, terpenoids were shown by violet bands, flavonoids by antimony (III) chloride gave bluish fluorescence, phenolics and polyphenols were shown by green bands (Ferric Chloride and Tin (IV) chloride respectively). The original plate distinguished the observations before and after spraying with the derivatization reagents.

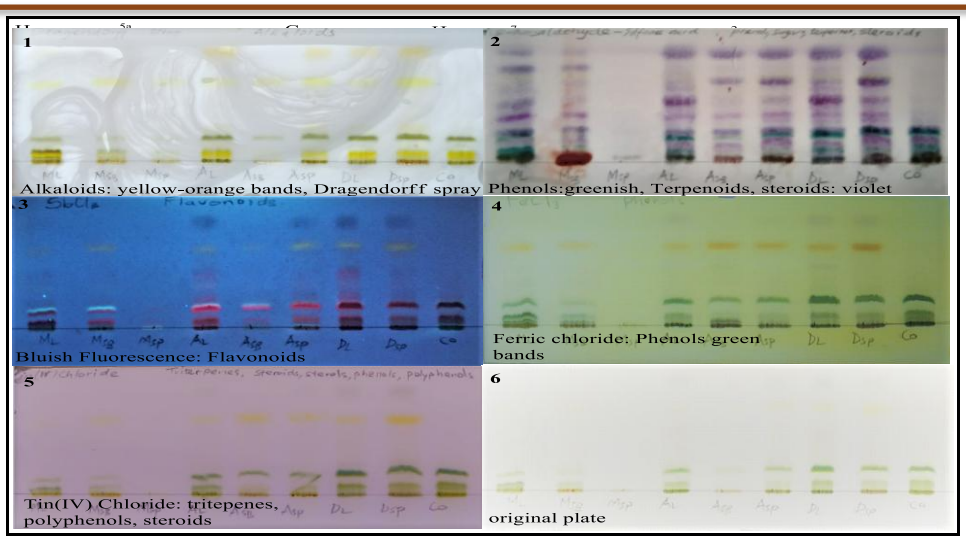

Figure 1. Phytochemical screening through TLC-DB method: 1. Yellow-orange bands (alkaloids), 2. Violet bands (terpenoids), 3. Bluish fluorescents (flavonoids), 4. Greenish bands (phenols/polyphenols), 5. Green bands (Polyphenols), 6. Original plate (For comparison).

Phytochemical content quantification results

Methanol extracts of the leaves had the highest total phenolic content (TPC) at 98 mg GAE/g. The DCM extracts of the seedpods showed the highest TPC at 102 mg GAE/g. The acetone extracts of the seedpods had the highest TPC at 151 mg GAE/g. For total alkaloidal content (TAC), the methanol extracts of the leaves had the highest TAC at 61 mg.

Table 1: UV-Vis spectrophotometric quantification of phytochemicals of *Senna didymobotrya*

Test/extract	MeOH leaf	MeOH seedpod	MeOH stembark	DCM leaf	DCM seedpod	DCM stembark	Acetone leaf	Acetone seedpod	Acetone stembark
TPC mg GAE/g	98±0.52	25±0.18	80±0.68	65±0.50	102±0.50	53±0.26	45±0.58	151±0.84	54±0.12
TAC (mg)	61±0.03	17±0.16	37±0.66	71±0.79	89±0.79	77±0.27	44±0.43	43±0.87	14±0.74
TTC mg/g	5±0.68	5±0.12	3±0.61	3±0.80	1±0.47	1±0.41	2±0.60	4±0.32	8±0.04

Key: TPC (Total phenol content), TAC (Total alkaloid content), TTC (Total terpenoid content).

The DCM extracts of the seedpods had the highest TAC at 89 mg, with the stem bark at 77 mg and the leaves at 71 mg. The acetone extracts of the leaves and seedpods had the highest TAC at 44 mg and 43 mg, respectively, followed by the stem bark at 14 mg. The total terpenoid content (TTC) for the methanol extracts of the leaves and seedpods had the highest TTC at 5 mg/g each, followed by the stem bark at 3 mg/g. The acetone extracts of the stem bark had the highest TTC at 8 mg/g, followed by the seedpods at 4 mg/g and the leaves at 2 mg/g as set in Table 1.

Direct bio-autographic bioassay results

The direct bio-autographic bioassay evaluated the plant's extract against gram-negative Salmonella typhimurium (ATCC-14028), Escherichia coli (ATCC-25922), Pseudomonas aeruginosa (ATCC-12903), and gram-positive Staphylococcus aureus (ATCC-25923). Staphylococcus aureus showed the highest zone of inhibition at a concentration of 500 mg/ml. The acetone leaf extract had an inhibition zone of 11±0.15 mm against S. aureus, while the stem bark

and seedpod extracts showed zones of 11±0.12 mm and 13±0.00 mm, respectively. Table 2 summarises the bioassay by giving the inhibition zones in mm.

Table 2: Results on bioautographic bioassay (p≥0.05)

Strain/extract	Acetone leaf	Acetone stembark	Acetone seedpod	DCM stembark	A1	A2	A3
E. coli	0	0	0	0	0	0	0
S. typhimurium	0	0	0	0	0	0	0
P. aeruginosa	0	11±0.00	12±0.10	11±0.17	11±0.10	12±0.15	9±0.12
S. aureus	11±0.15	11±0.12	13±0.00	0	7±0.06	10±0.06	0

Key: A1 = 1,8-dihydroxy-3-methoxy-6-methylanthracene-9,10-dione, A2 = 1,8-dihydroxy-3-methylanthracene-9,10-dione, A3 = 1, 5-dihydroxy-3-methylanthracene-9,10-dione

Compounds 1, 8-dihydroxy-3-methoxy-6-methylanthracene-9,10-dione and 1,8-dihydroxy-3-methylanthracene-9,10-dione also showed significant activity, with inhibition zones of 11±0.10 mm and 12±0.15 mm against P. aeruginosa while compound 1, 5-dihydroxy-3-methylanthracene-9,10-dione had the least effect, with a zone of 9±0.12 mm against P. aeruginosa. Compound 1, 8-dihydroxy-3-methylanthracene-9, 10-dione exhibited moderate activity with a zone of 10±0.06 mm against S. aureus.

Structure elucidation 1, 8-dihydroxy-3-methoxy-6-methylanthracene-9, 10-dione

1,8-dihydroxy-3-methoxy-6-methylanthracene-9,10-dione: Orange crystalline; TLC Rf :0.62 (70:30 DCM: Hexane), m.p. 128–129 °C; LC rt; 12.5 min ESI-MS m/z [M+H]+ 284.96 (calculated for C16H12O5, 284.96 [M+H]+); ^{1}H NMR (400 MHz, Chloroform-d) δ 12.32 (s, 1H), 12.13 (s, 1H), 7.63 (s, 1H), 7.37 (d, J = 2.5 Hz, 1H), 7.09 (s, 1H), 6.69 (d, J = 2.5 Hz, 1H), 3.94 (s, 4H), 2.45 (s, 4H). ^{13}C NMR (101 MHz, Chloroform-d) δ 190.82, 182.70, 166.56, 165.20, 162.51, 148.47, 135.26, 133.22, 124.53, 121.32, 113.68, 110.27, 108.25, 106.78, 56.11, and 22.19 ppm.

Table 3: ^{1}H and ^{13} NMR data for 1, 8-dihydroxy-3-methoxy-6-methylanthracene-9, 10-dione and its reference to the Physcion.

^{13}C NMR (ppm)	Carbon type	^{13}C NMR Physcion (ppm) [49]	^{1}H NMR 400 MHz, Chloroform-d	Chemical shifts (δ) ppm	Physcion; ^{1}H NMR (δ) [50]
22.19	(-CH3)	22.10	8-OH	12.32 (s)	12.30 (s)
56.11	-OCH3	56.05	1-OH	12.13 (s)	12.10 (s)
106.78	Caro	106.70	H-7	6.69 (s)	6.67 (s)
108.25	Caro	108.10	H-5	7.37(s)	7.35 (s)
110.27	Caro	110.20	H-4	7.63 (s)	7.61 (s)
113.68	Caro	113.60	H-2	7.09 (s)	7.06 (s)
121.32	Caro	121.20	3-OCH3	3.94 (s)	3.92 (s)
124.53	Caro	124.40	2-CH3	2.45 (s)	2.43 (s)
133.22	Caro	133.20			
135.26	Caro	135.20			
148.47	Caro	148.40			
162.51	-C=O	162.50			
165.20	-C=O	165.20			

166.56	-C=O	166.50
182.07	-C=O	181.90
190.82	-C=O	190.80

The ^{1}H NMR (400 MHz, Chloroform-d) showed proton signals at δ 12.32 (s, 1H, -OH), and 12.13 (s, 1H, -OH) characteristic of phenol protons, δ 7.63 (s, 1H, =CH), 7.37 (d, J = 2.5 Hz, 1H, =CH), 7.09 (s, 1H, =CH), 6.69 (d, J = 2.5 Hz, 1H, =CH) characteristic of aromatic protons and δ 3.94 (s, 4H, -OCH3) for methoxy and δ 2.45 (s, 4H, -CH3) deshielded methyl protons. The solvent peak (CDCl3) absorbed at δ 7.26 ppm for the ^{1}H NMR.

The ^{13}C NMR displayed 16 signals, ten quaternary carbons (-C) at δ 110.27, 113.68, 133.22, 135.26, 148.47, 162.51, 165.20, 166.56, 182.07, and 190.82. Carbon-13 NMR spectra also showed one methyl group (-CH3) at δ 22.19, one methoxy group (-OCH3) at δ 56.11, and four methine groups (-CH) at δ 106.78, 108.25, 121.32, and 124.53. The chemical shifts were evident of aromatic carbons (δ 148.47, 135.26, 133.22, 124.53, 121.32, 113.68, 110.27, 108.25, and 106.78 ppm), aliphatic carbons (δ 56.11 and 22.19 ppm), and carbonyl carbons (δ 190.82, 182.70, 166.56, 165.20, and 162.51 ppm). This suggested that the molecule contained aromatic rings that were consistent with UV-Visible data and substituted with methoxy groups (-OCH3) and carbonyl groups (-C=O). The solvent peak (CDCl3) absorbed at δ 76.84-77.48 for the carbon-13 NMR.

The methoxy group was assigned to C-15 based on the signal at δ 56.11 ppm, while the methyl carbon bonded to C-16 appeared at δ 22.19 ppm. The DEPT spectrum revealed the presence of either -CH, -CH2, or -CH3 non-quaternary carbons. The –CH/CH3 and CH2 were presented as either positive or negative peaks or vice versa in the DEPT spectrum depending on the operating frequency. The DEPT carbon-13 NMR was ran at a frequency of 135 MHz, a frequency that could detect all the –CH, -CH2, and –CH3 carbons. It showed six non-quaternary carbons (DEPT-135 MHz; δ 124.53, 121.32, 108.25, 106.78, 56.11, and 22.19 ppm). The observed peaks at δ 22.19 and 56.11 were identified as belonging to the Methyl (-CH3) and the methoxy group (-OCH3) respectively.

The HSQC revealed the direct attachment of the methyl proton at δ 2.45 ppm to C-3, while the singlets at δ 7.09 and 7.63 ppm corresponded to protons directly bonded to C-2 and C-4, respectively. The methoxy group was linked to C-6, with its protons directly bonded to C-15. Additionally, HSQC displayed a singlet proton at δ 7.37 ppm and another at δ 6.69 ppm, attached to C-5 and C-7 respectively. The two hydroxyl protons at δ 12.13 ppm and 12.32 ppm had an attachment to C-1 and C-8 respectively [Branco, A., et al.,2011, Mining, J., et al.,2014].

The HMBC analysis demonstrated correlations between protons and carbons that were two to three bonds away. The methyl protons at δ 2.45 ppm attached to C-16 had a bond correlation with C-3, C-2, and C-4. The proton at δ 7.63 ppm correlated with C-10, C-3, C-14, C-2, C-13, and C-16. The proton at δ 7.09 ppm had a bond correlation to C-4, C-13, and C-16. The proton at δ 7.37 ppm had a bond correlation with C-6, C-12, and C-5 while C-6, C-8, and C-5 were bond-correlating to the proton at δ 6.69 ppm. The methoxy protons at δ 3.94 ppm had a bond correlation to C-6. Furthermore, the hydroxyl (-OH) protons at δ 12.13 ppm and δ 12.32 ppm had a bond correlation to C-1, C-2, C-13, and C-8, C-12 respectively. The HMBC correlation for the atom connectivity proved an anthracene structure confirming the proposed structure in Figure 4.3. Following the ^{13}C NMR, and ^{1}H NMR data and based on the available spectral data from literature, the compound

corresponded to that of Physcion [Mari, S.H., et al.2019]. Table 4 shows the proton and carbon-13 data for 1,8-dihydroxy-3-methoxy-6-methylanthracene-9,10-dione with reference to Physcion.

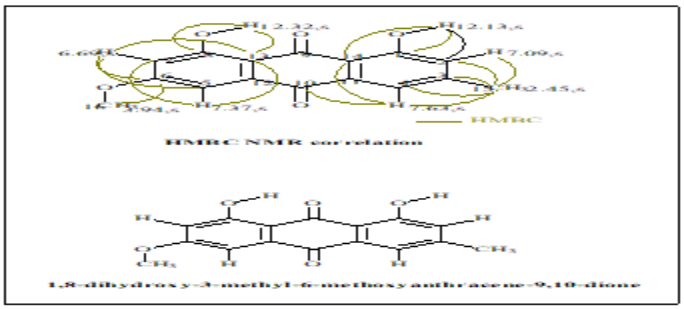

Figure 2. ^{1}H-^{13}C NMR correlation and structure of 1,8-dihydroxy-3-methoxy-6-methylanthracene-9,10-dione

The compound 1,8-dihydroxy-3-methoxy-6-methylanthracene-9,10-dione, displayed UV absorbance maxima (λ max) around 224, 268, 287, and 437 nm in acetone characteristic of the conjugated aromatic systems and polyenes [Pratiwi, R.A. and A.B.D. 2022,Ahluwalia, V.,2023]. Treatment of the prep-TLC plate with p-anisaldehyde-sulfuric acid produced a purple spot that subsequently turned greenish, characteristics of a phenolic compound. The ESI mass spectrometry analysis of 1,8-dihydroxy-3-methoxy-6-methylanthracene-9,10-dione revealed a base peak at [M+H] +, measuring 284.96 Da corresponding to that of Physcion. The other peaks were registered as a result of the different ionization that the molecule underwent giving isotopes and adducts of the identified molecule consistent with a molecular formula of C16H12O5 as depicted in Figure 3 (Weissberg, et al, 2011).

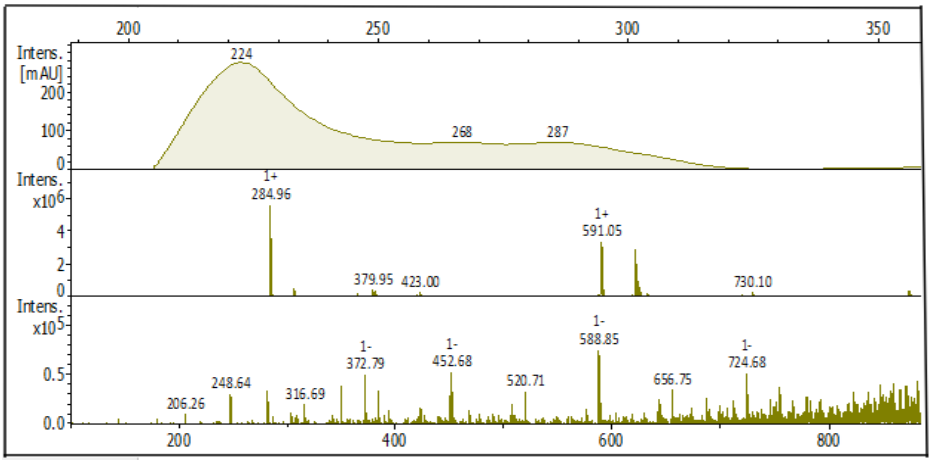

Figure 3. UV-vis and ESI-MS spectra for 1,8-dihydroxy-3-methoxy-6-methylanthracene-9,10-dione.

Structure elucidation of compound 1, 8-dihydroxy-3-methylanthracene-9, 10-dione

1, 8-dihydroxy-3-methylanthracene-9,10-dione: Orange-yellow crystals, TLC Rf :0.50 (70:30 DCM: Hexane), m.p. 190-191 oC, LC rt: 11.5 min, ESI-MS m/z [M+H]+ 254.93 (calculated for

C15H10O4, 254.93 [M+H]+); : ^{1}H NMR (400 MHz, Chloroform-d) δ 12.13 (s, 1H), 12.03 (s, 1H), 7.83 (d, J = 7.5 Hz, 1H), 7.69 (s, 0H), 7.68 – 7.65 (m, 2H), 7.30 (d, J = 8.4 Hz, 1H), 7.11 (s, 1H), 2.47 (s, 3H). ^{13}C NMR (101 MHz, Chloroform-d) δ 192.59, 182.07, 162.75, 162.45, 149.38, 136.99, 133.67, 133.31, 124.60, 124.41, 121.40, 119.97, 115.91, 113.77, and 22.30 ppm.

The ^{1}H-NMR (400 MHz, Chloroform-d) spectrum of compound 20 displayed two highly shielded peaks attribuTable to phenol protons at δ 12.13 (s, 1H, OH) and 12.03 (s, 1H, OH), aromatic protons at δ 7.83 (d, J = 7.5 Hz, 1H, =CH), 7.69 (s, 1H, =CH), 7.68 – 7.65 (m, 2H, CH), 7.30 (d, J = 8.4 Hz, 1H, =CH), 7.11 (s, 1H, =CH), and a deshielded methyl protons at δ 2.47 (s, 3H,-CH3). Further analysis revealed two doublets at δ 7.83 and δ 7.30, corresponding to aromatic protons linked to C-5 and C-7, respectively. A multiplet at δ 7.66 for the vicinal protons, which coupled with C-6, interacted with the protons on C-5 and C-7. Deuterated chloroform, with a peak at δ 7.26 ppm, was used as the solvent for the ^{1}H NMR analysis. The triplet at δ 7.66 ppm was due to the coupling with the protons at δ 7.29 and 7.83 ppm.

The ^{13}C NMR spectrum of compound 20 (101 MHz, Chloroform-d) displayed chemical shifts at δ 192.59, 182.07, 162.75, 162.45, 149.38, 136.99, 133.67, 133.31, 124.60, 124.41, 121.40, 119.97, 115.91, 113.77, and 22.30 ppm. The ^{13}C NMR and DEPT spectra indicated a total of fifteen carbon atoms. Evaluation of ^{13}C NMR data indicated the presence of methine carbons characteristic of aromatic systems. The analysis revealed nine quaternary carbons (C), five trivalent methine groups (=CH-), and one methyl group (-CH3). The carbon peak corresponding to a methyl carbon attached to C-3 was observed at δ 22.30 ppm. The methine carbons exhibited chemical shifts at δ 136.99 (C-4), δ 121.40 (C-6), δ 124.41 (C-2), δ 119.97 (C-5), and δ 124.60 (C-7) typical of aromatic carbons.

Table 4: ^{1}H and Carbon-13 NMR data for 1, 8-dihydroxy-3-methylanthracene-9,10-dione and its relation to Chrysophanol

^{13}C NMR in ppm	Type of carbon	^{13}C NMR Chrysophanol in ppm [49, 56]	Chemical shifts (δ)	Chrysophanol ^{1}H NMR (δ) [50, 56]
22.30	Me (CH3)	22.20	12.13 (s)	12.11 (s)
113.77	Caro	113.70	12.03 (s)	12.00 (s)
115.91	Caro	115.80	7.83 (d, J = 7.5 Hz)	7.81 (d)
119.97	Caro	119.90	7.68 – 7.65 (m),	7.64 (t)
121.40	Caro	121.30	7.69 (s)	7.65 (s)
124.41	Caro	124.30	7.30 (d, J = 8.4 Hz)	7.29 (d)
124.60	Caro	124.50	7.11 (s)	7.09 (s)
133.31	Caro	133.30	2.47 (s)	2.45 (s)
133.67	Caro	133.60		
136.99	Caro	136.90		
149.38	Caro	149.30		
162.45	C=O	162.40		
162.75	C=O	162.70		
182.07	C=O	181.90		
192.59	C=O	192.50		

Other signals exhibited at δ 192.59 (C-9), δ 182.07 (C-10), δ 162.75 (C-1), δ 162.45 (C-8), δ 149.38 (C-3), δ 133.67 (C-14), δ 133.31 (C-11), δ 115.91 (C-12), and δ 113.77 (C-13), corresponding to the nine quaternary carbons. The highest chemical shifts at δ 192.59 (C-9) and δ 182.07 (C-10) indicate that these ketone carbons were aromatic. The summary of the ^{13}C DEPT-135 NMR data for compound 20 included δ 136.99, 124.60, 124.41, 121.40, and 119.97 for CH, and 22.30 as a CH3 peak.

The HMBC data indicated the proton at δ 7.69 ppm assigned to C-4 which correlated with carbons C-14 and C-2. The proton registered as a multiplet at δ 7.66 ppm on (C-6) had an association with C-8 and C-11. The doublet at δ 7.29 ppm correlated with carbons labelled C-5 and C-12, and the other doublet at δ 7.83 ppm linked with carbons labelled C-7 and C-12. The methyl protons at δ 2.47 ppm correlated with carbons labelled C-2 and C-3. The OH protons also showed a correlation with the carbons, where the OH proton at δ 12.13 ppm linked to carbons labelled C-12 and C-7, while the OH proton at δ 12.03 ppm linked to C-13, C-2, and C-1.

The correlation spectroscopy (1H-1H COSY) spectra showed a correlation of neighbouring protons that had coupling effects on each other. The triplet at δ 7.66 ppm was correlated with protons at δ 7.83 ppm and 7.29 ppm, hence registering as a triplet due to the coupling effects of the respective neighbouring ortho protons. Similarly, the protons at δ 7.29 ppm and 7.83 ppm were displayed as doublets, as each was adjacent to the proton at δ 7.66 ppm from opposite sides. The HSQC NMR data showed that the aromatic protons with chemical shifts at δ 7.11, 7.69, 7.83, 7.66, and 7.29 ppm were directly attached to C-2, C-4, C-5, C-6, and C-7, respectively. The methyl protons (δ 2.47) were bonded to C-3.

The ^{13}C and ^{1}H NMR chemical shifts together with the correlations from HMBC, HSQC, and COSY gave the compound 1, 8-dihydroxy-3-methylanthracene-9,10-dione which was identified as Chrysophanol, an anthraquinone derivative with the chemical formula C15H10O4 [Mari, S.H., et al.,2019, Prateeksha, et al.,2019].

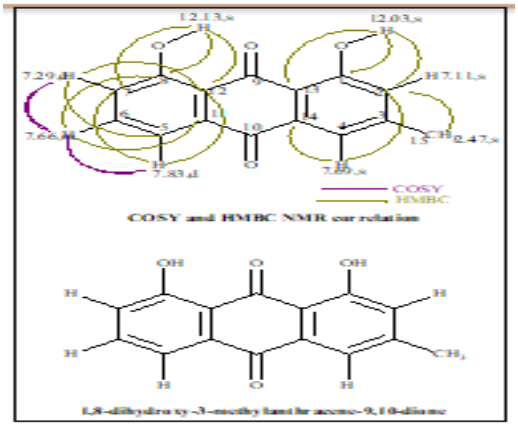

Figure 4. Structure of 1, 8-dihydroxy-3-methylanthracene-9, 10-dione and the ^{1}H-^{13}C NMR correlations

The compound 1, 8-dihydroxy-3-methylanthracene-9,10-dione displayed UV absorbance maxima (λ max) around 200, 225, 259, 280, 288, and 429 nm in acetone typical of conjugated aromatic systems. The distinct absorbance peaks were useful for differentiating between the two anthraquinone derivatives. Both compounds exhibited similar UV absorption characteristics, particularly in the UV region around 224-225 nm, and 287-288 nm which are typical for

anthraquinones due to their conjugated systems. The absorption around 430 nm indicates their potential to absorb visible light, contributing to their colour. These UV maxima values were significant for differentiating these compounds thus aiding in their analysis in structural studies. The Electrospray Ionization Mass Spectrometry (ESI-MS) analysis of compound 1, 8-dihydroxy-3-methylanthracene-9,10-dione displayed the highest mass peak at m/z 254.93 Da corresponding to molecular ion peak of [M+H] + [Prateeksha, et al.,2019, Onoda, T., et al.,2016] as depicted in Figure 5 below.

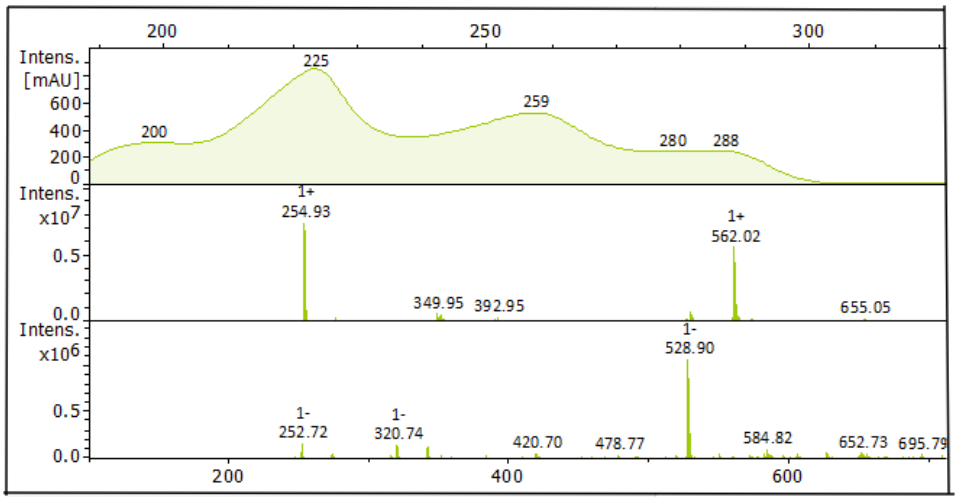

Figure 5. UV-vis and ESI-MS spectra for compound 1, 8-dihydroxy-3-methylanthracene-9, 10-dione.

Structure elucidation of compound 1, 5-dihydroxy-3-methylanthracene-9, 10-dione

1,5-dihydroxy-3-methylanthracene-9,10-dione: Reddish-brown crystals, TLC Rf 0.46 (70:30 DCM: Hexane), m.p. 189-190 oC; ESI-MS m/z [M+H]+ 254.96 (calculated for C15H10O4, 254.72 [M+H]+); ^{1}H NMR (400 MHz, Acetone-d6) δ 12.06 (s, 1H), 11.97 (s, 1H), 7.83-7.85 (m, J = 7.8, 2H), 7.80 (d, J = 1.4 Hz, 1H), 7.63 (s, 1H), 7.36 (dd, J = 1.5 Hz, 1H), 7.20 (s, 1H) 2.50 (s, 4H). ^{13}C NMR (101 MHz, Chloroform-d) δ 182.34, 182.10, 163.28, 163.05, 150.69, 137.36, 134.57, 124.94, 124.71, 121.69, 121.50, 120.34, 116.68, 114.60, and 22.05 ppm.

The ^{1}H NMR (400 MHz, Acetone-d6) signals observed were at δ 12.06 (s, 1H, -OH), 11.97 (s, 1H, -OH) for phenol protons, 7.83-7.85 (m, J = 7.8, 2H, -CH), 7.80 (d, J = 1.4 Hz, 1H, -CH), 7.63 (s, 1H, -CH), 7.36 (dd, J = 1.5 Hz, 1H, -CH), 7.20 (s, 1H, =CH) aromatic protons, 2.50 (s, 4H, -CH3) deshielded methyl protons.

Table 5: ^{1}H and ^{13}C NMR data for 1, 5-dihydroxy-3-methylanthracene-9, 10-dione.

^{13}C NMR	Type of carbon	^{13}C NMR from Literature [59, 60]	^{1}H NMR400 MHz, Acetone-d6,	Proton from literature [59, 60]
22.05	Me (-CH3)	22.2	12.06 (s)	12.13 (s)
114.60	Caro	113.7	11.97 (s)	12.03 (s)
116.68	Caro	116.0	7.83-7.85 (m, J = 7.8)	7.83 (dd)
120.34	Caro	119.9	7.80 (d, J = 1.4 Hz)	7.68 (d)
121.50	Caro	121.3	7.63 (s)	7.68 (s)

121.69	Caro	124.3	7.36 (dd, J = 1.5 Hz)	7.31 (dd)
124.71	Caro	124.5	7.20 (s)	7.03 (s)
124.94	Caro	127.3	2.50 (s)	2.48 (s)
134.57	Caro	133.2		
137.36	Caro	136.9		
150.69	Caro	149.3		
163.05	C=O	162.4		
163.28	C=O	162.7		
182.10	C=O	192.3		
182.34	C=O	192.4		
206.10	Deutacetone			

The ^{1}H NMR spectrum displayed characteristic signals for phenol and aromatic protons, with the phenol protons resonating downfield and the aromatic protons appearing in the region of 6.0 to 8.0 ppm. Further analysis revealed two singlets for aromatic protons linked to C-2 and C-4 at δ 7.20 ppm and δ 7.63 ppm, respectively. Additionally, three other singlets were observed: a methyl singlet at δ 2.50 ppm and two for the phenol protons at δ 12.06 ppm and 11.97 ppm. The signal for deuterated acetone showed a quintet with a splitting of about 2 Hz, recorded at δ 2.05 ppm.

The ^{13}C NMR spectrum (101 MHz, Acetone-d6) displayed chemical shifts at δ 182.34, 182.10, 163.28, 163.05, 150.69, 137.36, 134.57, 124.94, 124.71, 121.69, 121.50, 120.34, 116.68, 114.60, and 22.05 ppm. Evaluation of ^{13}C NMR data indicated the presence of methine carbons characteristic of aromatic systems. Nine quaternary carbons (C), five trivalent methine groups (=CH-), and one methyl group (-CH3). The carbon signal at δ 22.05 ppm was assigned to C-15, corresponding to the methyl group. The methine carbons were identified at δ 137.36 ppm (C-7), δ 124.94 ppm (C-6), δ 124.71 ppm (C-2), δ 121.50 ppm (C-4), and δ 120.34 ppm (C-8).

The nine quaternary carbons exhibited shifts at δ 182.34 ppm (C-9), δ 182.10 ppm (C-10), δ 163.28 ppm (C-1), δ 163.05 ppm (C-5), δ 150.69 ppm (C-3), δ 134.57 ppm (C-12), δ 121.69 ppm (C-14), δ 116.68 ppm (C-11), and δ 114.60 ppm (C-13), indicating the presence of olefin or aromatic carbons, with the highest shifts attributed to the ketone carbons. An intense peak at δ 206.10 ppm was attributed to the solvent, deuterated acetone (CD3COCD3), with the carbonyl carbon (C=O) appearing around 206.10 ppm and the methyl carbon (-CD3) around 29.8 ppm. The data was consistent with that obtained from literature. The proton and carbon-13 NMR data corresponded to literature reported from Rumex dentatus [Kazmi, M., et al., 2006, Mohamed, N.Z., et al.,2014].

The correlation spectroscopy (COSY) spectra demonstrated correlations between neighbouring protons with coupling effects. The multiplet at δ 7.83 ppm was correlated with protons at δ 7.80 ppm and 7.37 ppm. Similarly, the protons at δ 7.37 ppm and 7.80 ppm were recorded as doublets, each neighbouring the proton at δ 7.83 ppm from opposite sides.

The correlation for HMBC showed that the proton at C-2 (δ 7.20 ppm) correlated with C-1, C-13, C-15, and C-4. The proton at C-4 (δ 7.63 ppm) correlated with C-10, C-15, C-2, and C-13. The directly attached protons of C-15 (δ 2.50 ppm) correlated with C-4 and C-2 whereas the doublet attached to C-8 (δ 7.80 ppm) correlated with C-12, C-9, C-11, C-7, and C-6. The other doublet attached to C-6 (δ 7.36 ppm) correlated with C-5, C-11, and C-8. The multiplet proton bonded to C-7 (δ 7.83 ppm) correlated with C-5.

The HSQC analysis indicated that the methyl proton at δ 2.50 ppm bonded to C-15 (δ 22.05 ppm). The singlets at δ 7.63 ppm and δ 7.20 ppm corresponded to protons directly bonded to C-4

(δ 121.50 ppm) and C-2 (δ 124.71 ppm), respectively. Other aromatic protons showed a doublet at δ 7.80 ppm in (δ 120.34 ppm) and δ 7.36 ppm in (δ 124.94 ppm), associated with protons attached to C-8 and C-6, respectively. The multiplet at δ 7.83 ppm was directly bonded to C-7 (137.36 ppm).

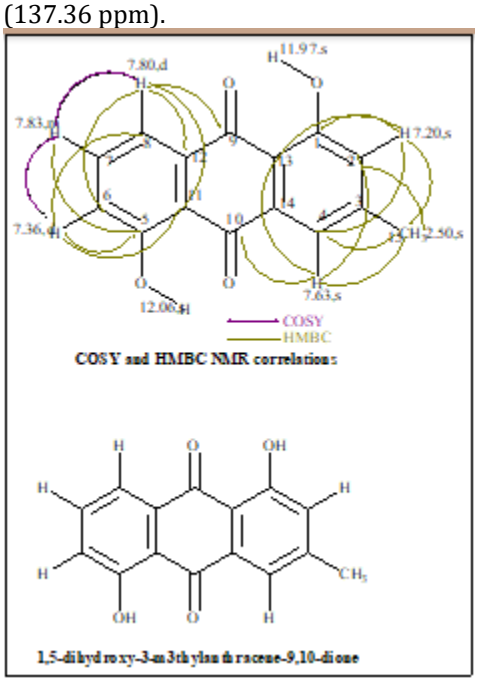

Figure 6. Compound 1, 5-dihydroxy-3-methylanthracene-9, 10-dione and its NMR correlation

DISCUSSION

The TLC-DB method clearly showed the active metabolites in the *S. didymobotrya* plant as a good candidate for inhibiting bacterial infections. Different colours and fluorescence under UV light identified alkaloids, phenolics, terpenoids, and flavonoids. However, phenolics were detected in every part of the plant used. This mixture of metabolites explains why the plant has a long historical use in ethno medicine. The findings substantiate the existing literature, which also indicates that phenolic anthraquinones are the primary components in the Senna family (Sadiaet al., 2022; Jeruto et al., 2016; Anthoney et al., 2014).

The total phenolic content, total alkaloid content, and total terpenoid content of the plant were quantified. It was expected that the TTC content to be higher than other phytochemical due to the strong aroma of the plant that was always associated with low molecular weight terpenes. However, the low TTC content was validated as a result of the low molecular weight terpenes being so much volatile. A special technique of capturing and analysing the low molecular weight terpenes such as GC-MS would be the best recommendation for their analysis. Furthermore, the variations in phytochemical contents among the different extracts and plant parts was an indication that the choice of solvent and the plant part was crucial for a targeted extraction of specific compounds for further research and potential applications (Sadia et al., 2022; Anthoney et al., 2014; Jeruto et al., 2016; Granda-Santos et al., 2025; Hübschmann, 2025).

The TLC-DB provided the argument into the antimicrobial properties of the plant extracts against bacterial strains. Both E. coli and S. typhimurium were resistant to all tested extracts and

compounds. The Gram-negative bacteria were argued to be less vulnerable to antibiotic treatments due to their having exceptional structural and functional features. Their outer membrane acts as a strong permeability blockade, stopping many other antibiotics from entering the cell. The robustness of the cell was argued to be one of the factors facilitating their resistance to antibiotics (Ghai and Ghai, 2018; Garcia et al., 2012; Nikaido, 2022). These basic mechanisms, combined with the ability to obtain resistance genetic material through gene transfer, make Gram-negative bacteria particularly challenging to treat (Vergalli et al., 2020; Gauba, 2023).

On the other hand, the Gram-positive bacterium, S. aureus showed significant weakness to the extracts. Gram-positive bacteria are generally more susceptible to antibiotic treatments than Gram-negative bacteria due to their simpler cell envelope structure and lack of an outer membrane. The thick peptidoglycan layer in Gram-positive bacteria is highly accessible to antibiotics such as β-lactams, which target to inhibit the peptidoglycan synthesis, leading to cell wall disruption and death of the bacteria (Rajagopal, 2017; Jubeh et al., 2020).

1, 8-dihydroxy-3-methoxy-6-methylanthracene-9, 10-dione was isolated as an orange crystalline solid (Mpt=128-129 °C, ESI-MS=284.96 Da, LC rt=12.5 mins, UV acetone λmax= 224, 268, 287, 437 nm) characteristic conforming to conjugated aromatic systems and polyenes (Pratiwi, 2022; Ahluwalia, 2023). Literature mention the retention time for the elucidated compound to usually range between 4 to about 20 minutes. However, the presence of the hydroxyl, the carboxyl and other functional groups could affect the retention time by changing the way the compounds interact with the stationary phase (Liu et al., 2015). The identity of 1,8-dihydroxy-3-methoxy-6-methylanthracene-9,10-dione was further confirmed through spectroscopic data from ^{1}H, ^{13}C, DEPT, HSQC, COSY, NOESY, and HMBC experimentations. The data conformed to Physcion, an anthraquinone derivative with the molecular formula C16H12O5 (Kiprotich, 2013; Wang et al., 2023; Luyen, 2019). Physcion is recognized for its medicinal benefits, showing varied pharmacological properties comprising anticancer, antimicrobial, antifungal, anti-inflammatory, antioxidant, hepatoprotective, antiviral, and anti-diabetic effects. These properties amongst others underscore its therapeutic potential across various medical applications (Prateeksha et al., 2019; Adnan et al., 2021; Liu et al., 2019; Huang et al., 2021; Dave and Ledwani, 2012).

1, 8-dihydroxy-3-methylanthracene-9,10-dione was isolated as orange-yellow crystals (Mpt=190-191 °C, ESI-MS=254.72 Da, LC rt =11.5 mins, UV acetone λmax= 200, 225, 259, 280, 288, 429 nm). The compounds exhibited similar UV absorption characteristics, particularly in the UV region around 224-225 nm, and 287-288 nm which were characteristic for anthraquinones due to their having a conjugated system. The absorption around the wavelength of 430 nm indicated the potential of the molecules to absorbing visible light hence, contributing to their colour and bioactivity (Prateeksha et al., 2019). 1,8-dihydroxy-3-methoxy-6-methylanthracene-9,10-dione (Physcion) and 1, 8-dihydroxy-3-methylanthracene-9,10-dione (Chrysophanol) exhibited similar retention times in liquid chromatography due to their structural similarities and chemical properties. Both of the compounds belonged to the anthraquinone family, possessing similar hydrophobic characteristics that lead to similar interactions with the stationary phase during chromatography. Furthermore, the optimization of the chromatographic conditions, such as the choice of mobile phase and column type, could have resulted in an overlapping of the retention times for these compounds. This resemblance could complicate their separation, leading to occasions where they would elute at nearly the same time under specific analytical conditions (Feng et al., 2016; Škalameraet al., 2017)

Similarly, Chrysophanol (1, 8-dihydroxy-3-methylanthracene-9, 10-dione) demonstrates a broad spectrum of medicinal properties. The medicinal properties included antimicrobial, antifungal, hepatoprotective, antidiabetic, neuroprotective, and laxative effects. These properties highlighted its significance in both traditional and modern medicine (Dave and Ledwani, 2012). These results were crucial for understanding the chemical behaviour and potential biological activities of 1,8-dihydroxy-3-methoxy-6-methylanthracene-9,10-dione and 1, 8-dihydroxy-3-methylanthracene-9,10-dione in various applications such as pharmacological uses.

1,5-dihydroxy-3-methylanthracene-9,10-dione was isolated as reddish-brown crystals (Mpt=189-190 oC, Rf=0.46, UV λmax =224, 257, 429 nm). Its identity was confirmed by correlating all its NMR data (^{1}H, ^{13}C, DEPT, HSQC, and HMBC) with references from literature.. Based on the information and verifying with literature data, 1,5-dihydroxy-3-methylanthracene-9,10-dione was identified as a protonated 1, 5- and 1, 8-dihydroxyanthraquinones tautomer. Tautomers are fast interconvertible structural isomers. They usually differ by the position of a hydrogen atom and a double bond and exist in dynamic equilibrium (Korth and Mulder, 2013). Their interconversion plays a vital role in organic and biological chemistry. The compound 1, 5-dihydroxy-3-methylanthracene-9, 10-dione also belonged to the anthraquinone family.

Anthraquinones are known for their diverse biological activities and applications in the various fields, including medicine and dye production. Like many anthraquinones, 1, 5-dihydroxy-3-methylanthracene-9, 10-dione, exhibits antioxidant properties that can help reduce oxidative stress in biological systems. Although specific studies on this compound are limited, anthraquinones are traditionally recognized for their laxative properties, suggesting this compound may contribute to gastrointestinal health (Yagi et al., 2013; Fainet al., 2006). Due to its bioactivity, it is considered for use in phytotherapy, particularly in formulations aimed at treating various ailments, including tumour cancer (Adnan et al., 2021).

CONCLUSION

The compounds 1, 8-dihydroxy-3-methoxy-6-methylanthracene-9, 10-dione; 1, 8-dihydroxy-3-methylanthracene-9, 10-dione, and 1, 5-dihydroxy-3-methylanthracene-9, 10-dione were isolated from the plant. Compound 1, 5-dihydroxy-3-methylanthracene-9, 10-dione was identified for the first time in S. didymobotrya . However, it had been isolated from Rumex dentatus and Artemisia indica. The compounds exhibited efficacy against life-threatening pathogens like Pseudomonas aeruginosa. This informed its use could reduce the reliance on conventional antibiotics and mitigate resistance development. All the isolated compounds showed antibacterial inhibition exclusively against P. aeruginosa and S. aureus.

The TLC direct bioautography method allowed for simultaneous separation and biological testing on the same plate, making it a powerful tool for identifying antimicrobial properties in complex mixtures. This method was advantageous because it combined chromatographic separation with biological activity detection, allowing researchers to identify which components were responsible for antimicrobial effects without extensive preliminary purification steps. These findings provide a basis for the plant's antibacterial properties and open avenues for further pharmacological studies.

RECOMMENDATION

Future studies should examine the toxicity and in-vivo antibacterial properties of the isolated compounds and their applicability in drug designs as this study was limited to the in-vitro applications. Moreover, the combination of conventional antibiotics and the anthraquinones may also be ideal in understanding the synergistic effects and structural-activity evaluation studies of the compounds. However, HPTLC, enzyme, and ultrasound assisted extraction methods need to be employed to enhance on yield, specificity, and selectivity of phytochemicals.

Acknowledgment

We acknowledge the support of the Royal Society of Chemistry (RSC), UK, under Project Number R21-2274244013, which has been instrumental in advancing this research.

Disclosure statement

No potential conflict of interest was reported by the authors.

REFERENCE

Diab, M.A., of Genus Senna. 2024.

Khadhum, S.M. and K.A.A. Shaheed. Molecular Study of the Two Species of senna L. in Iraq. in IOP Conference Series: Earth and Environmental Science. 2025. IOP Publishing.

Osunga, S., et al., Ethnobotany of some members of the genus Cassia (Senna). Int J Novel Res Life Sci, 2023. 10(5): p. 1-14.

Sadia, B., J. Cherutoi, and C. Achisa, Phytochemical screening, total phenolic and flavonoid content of *Senna didymobotrya* , in Advances in Phytochemistry, Textile and Renewable Energy Research for Industrial Growth. 2022, CRC Press. p. 150-156.

Weldemariam, E.C. and S.W. Dejene, Predicting invasion potential of *Senna didymobotrya* (Fresen.) Irwin & Barneby under the changing climate in Africa. Ecological Processes, 2021. 10: p. 1-10.

Alemayehu, I., et al., Phytochemical analysis of the roots of *Senna didymobotrya* . Journal of Medicinal Plants Research, 2015. 9(34): p. 900-907.

Murdani, C.R., et al., Extraction, Synthesis and Derivatization of Emodin: An Overview. International Journal of Agriculture and Biology, 2024. 32(4): p. 315-332.

Qun, T., et al., Antibacterial activities of anthraquinones: structure–activity relationships and action mechanisms. RSC Medicinal Chemistry, 2023. 14(8): p. 1446-1471.

Raghuveer, D., et al., Exploring anthraquinones as antibacterial and antifungal agents. ChemistrySelect, 2023. 8(6): p. e202204537.

Havelikar, U., et al., Understanding quinone derivatives antibacterial and antimicrobial activities relies on the structural activity relationship, in Quinone-Based Compounds in Drug Discovery. 2025, Elsevier. p. 55-81.

Saleem, M., et al., Antibiotics overuse and bacterial resistance. Annals of Microbiology and Research, 2019. 3(1): p. 93-99.

Odonkor, S.T. and K.K. Addo, Bacteria resistance to antibiotics: recent trends and challenges. Int J Biol Med Res, 2011. 2(4): p. 1204-1210.

McEwen, S.A. and P.J. Collignon, Antimicrobial resistance: a one health perspective. Antimicrobial resistance in bacteria from livestock and companion animals, 2018: p. 521-547.

Olofinsan, K.A., H. Abrahamse, and B.P. George, Anti-proliferative and photodynamic activities of *Senna didymobotrya* (Fresen.) leaf alkaloid-rich extracts against breast cancer cells. BMC Complementary Medicine and Therapies, 2025. 25(1): p. 1-13.

Aminov, R., History of antimicrobial drug discovery: Major classes and health impact. Biochemical pharmacology, 2017. 133: p. 4-19.

Li, B. and T.J. Webster, Bacteria antibiotic resistance: New challenges and opportunities for implant-associated orthopedic infections. Journal of Orthopaedic Research®, 2018. 36(1): p. 22-32.

Organization, W.H., Monitoring global progress on antimicrobial resistance: tripartite AMR country self-assessment survey (TrACSS) 2019–2020: global analysis report. 2021: Food & Agriculture Org.

WHO-Group, Discovery, research, and development of new antibiotics: the WHO priority list of antibiotic-resistant bacteria and tuberculosis. The Lancet Infectious Diseases, 2018. 18(3): p. 318-327.

WHO, WHO global strategy for containment of antimicrobial resistance, in The Lancet Infectious Diseases. 2001, World Health Organization. p. 1-105.

WHO, Monitoring global progress on antimicrobial resistance: tripartite AMR country self-assessment survey (TrACSS) 2019–2020: global analysis report. 2021: Food & Agriculture Org.

WHO, WHO global strategy for containment of antimicrobial resistance. 2001, World Health Organization. p. 31-47.

Organization, W.H., A global health strategy for 2025-2028-advancing equity and resilience in a turbulent world: fourteenth General Programme of Work. 2025: World Health Organization.

Viertel, T.M., K. Ritter, and H.-P. Horz, Viruses versus bacteria—novel approaches to phage therapy as a tool against multidrug-resistant pathogens. Journal of Antimicrobial Chemotherapy, 2014. 69(9): p. 2326-2336.

Kortright, K.E., et al., Phage therapy: a renewed approach to combat antibiotic-resistant bacteria. Cell host & microbe, 2019. 25(2): p. 219-232.

Pulingam, T., et al., Antimicrobial resistance: Prevalence, economic burden, mechanisms of resistance and strategies to overcome. European Journal of Pharmaceutical Sciences, 2022. 170(11): p. 103-106.

Latolla, N., et al., Phytochemical composition and antidiabetic potential of the leaf, stem, and rhizome extracts of Cissampelos capensis Lf. South African Journal of Botany, 2023. 163(4): p. 468-477.

Laxminarayan, R., et al., The Lancet Infectious Diseases Commission on antimicrobial resistance: 6 years later. The Lancet Infectious Diseases, 2020. 20(4): p. 51-60.

Nyamwamu, B.L., et al., Phytochemical constituents of *Senna didymobotrya* Fresen irwin roots used as a traditional Medicinal plant in Kenya. 2015. 2(12): p. 2-7.

Shaikh, J.R. and M. Patil, Qualitative tests for preliminary phytochemical screening: An overview. International journal of chemical studies, 2020. 8(2): p. 603-608.

Febrina, L., B.D. Hikmawan, and M.D. Adyma, Secondary Metabolite Profiles and Antibacterial Activity of Mitragyna speciosa Leaf Extracts According to Vein Color Variation. Journal of Pharmaceuticals and Natural Sciences, 2025. 2(3): p. 109-118.

Athipornchai, A. and K. Klangmanee, A rapid determination of the effective antioxidant agents using their Fe (III) complexes. Arabian Journal of Chemistry, 2021. 14(3): p. 102986.

Afrokh, M., et al., Phytochemical screening and in vitro antioxidant activities of Mentha suaveolens Ehrh. extract. International Journal of Secondary Metabolite, 2023. 10(3): p. 332-344.

Ranaweera, C., et al., Phytochemical Testing Methodologies and Principles for Preliminary Screening/Qualitative Testing. 2024.

Tabasum, S., S. Khare, and K. Jain, Spectrophotometric quantification of total phenolic, flavonoid, and alkaloid contents of Abrus precatorius L. seeds. Asian J Pharm Clin Res, 2016. 9(2): p. 371-374.

Sánchez-Rangel, J.C., et al., The Folin–Ciocalteu assay revisited: improvement of its specificity for total phenolic content determination. Analytical methods, 2013. 5(21): p. 5990-5999.

Aryal, S., et al., Total phenolic content, flavonoid content and antioxidant potential of wild vegeTables from Western Nepal. Plants, 2019. 8(4): p. 90-96.

Lamuela-Raventós, R.M., Folin–Ciocalteu method for the measurement of total phenolic content and antioxidant capacity. Measurement of antioxidant activity & capacity: recent trends and applications, 2018: p. 107-115.

Malik, S., Qualtitative and quantitative estimation of terpenoid contents in some important plants of Punjab, Pakistan. Pakistan Journal of Science, 2017. 69(2).

Pedersen, D.S., et al., Quantitative analysis of geraniol, nerol, linalool, and α-terpineol in wine. Analytical and bioanalytical chemistry, 2003. 375(6): p. 517-522.

Korir, R.K., Evaluation of antimicrobial properties of medicinal plants used among the kipsigis community in Kenya. 2012.

Swargiary, G., et al., Molecular approaches to screen bioactive compounds from medicinal plants. Plant-Derived Bioactives: Production, Properties and Therapeutic Applications, 2020: p. 1-32.

AMUTHA, J. and S. GARAPATI, Tlc-Bioautography-Guided Antimicrobial Activity and Characterization of Active Compound of Schouwia Purpurea (Frossk.) Schweinf.

Bunya, S.R. and S. Lihan, Thin Layer Chromatography-Direct Bioautography and Identification of Compounds from the Semi-purified Fraction of Senna alata (Linn.). Tropical Journal of Natural Product Research, 2025. 9(8).

Choma, I.M. and W. Jesionek, TLC-direct bioautography as a high throughput method for detection of antimicrobials in plants. Chromatography, 2015. 2(2): p. 225-238.

Šegan, S., et al., Thin-layer chromatography in bioassays of antimicrobial compounds from plants. Journal of Liquid Chromatography & Related Technologies, 2021. 44(9-10): p. 507-518.

Botros, L., et al., Connecting the practice of modern qualitative and quantitative NMR analysis with its theoretical foundation. Journal of Natural Products, 2025. 88(3): p. 877-888.

Drevet Mulard, E., et al., Quantitative nuclear magnetic resonance for small biological molecules in complex mixtures: Practical guidelines and key considerations for non-specialists. Molecules, 2025. 30(8): p. 1838.

Giraudeau, P., Quantitative NMR spectroscopy of complex mixtures. Chemical Communications, 2023. 59(44): p. 6627-6642.

Mining, J.K., Bioactive metabolites of selected kenyan plants used as biopesticides against Acanthoscelides obtectus in Bungoma district, Kenya. 2014.

Mari, S.H., et al., Solvent-dependent structures of natural products based on the combined use of DFT calculations and ^{1}H-NMR chemical shifts. Molecules, 2019. 24(12): p. 22-90.

Branco, A., et al., Anthraquinones from the bark of Senna macranthera. Anais da Academia Brasileira de Ciências, 2011. 83(31): p. 1159-1164.

Mining, J., et al., Bioactive metabolites of *Senna didymobotrya* used as biopesticide against Acanthoscelides obtectus in Bungoma, Kenya. 2014. 5(16): p. 12-31.

Pratiwi, R.A. and A.B.D. Nandiyanto, How to read and interpret UV-VIS spectrophotometric results in determining the structure of chemical compounds. Indonesian Journal of Educational Research and Technology, 2022. 2(1): p. 1-20.

Ahluwalia, V., Ultraviolet Spectroscopy, in Instrumental Methods of Chemical Analysis. 2023, Springer. p. 233-269.

Weissberg, A. and S. Dagan, Interpretation of ESI (+)-MS-MS spectra—Towards the identification of "unknowns". International Journal of Mass Spectrometry, 2011. 299(2-3): p. 158-168.

Prateeksha, et al., Chrysophanol: a natural anthraquinone with multifaceted biotherapeutic potential. Biomolecules, 2019. 9(2): p. 68.

Prateeksha, et al., Chrysophanol: a natural anthraquinone with multifaceted biotherapeutic potential. Biomolecules, 2019. 9(2): p. 56-68.

Onoda, T., et al., Identification and evaluation of magnolol and chrysophanol as the principle protein tyrosine phosphatase-1B inhibitory compounds in a Kampo medicine, Masiningan. Journal of Ethnopharmacology, 2016. 186: p. 84-90.

Kazmi, M., et al., Phytochemistry and Bioactivity of Cassia Italica. 2006.

Mohamed, N.Z., et al., CCl4-induced hepatonephrotoxicity: protective effect of nutraceuticals on inflammatory factors and antioxidative status in rat. Journal of applied pharmaceutical science, 2014. 4(2): p. 87.

Anthoney, S.T., et al., Evaluation of in vitro antibacterial activity in *Senna didymobotrya* roots methanolic-aqua extract and the selected fractions against selected pathogenic

microorganisms. International Journal of Current Microbilology and Applied Sciences 2014. 3(5): p. 362-376.

Jeruto, P., et al., In vitro antifungal activity of methanolic extracts of different *Senna didymobotrya* (fresen.) HS Irwin & barneby plant parts. African Journal of Traditional, Complementary and Alternative Medicines, 2016. 13(6): p. 168-174.

Granda-Santos, M., et al., Characterization of Terpenoids in Aromatic Plants Using Raman Spectroscopy and Gas Chromatography–Mass Spectrometry (GC–MS). International Journal of Molecular Sciences, 2025. 26(23): p. 11254.

Hübschmann, H.-J., Handbook of GC-MS: fundamentals and applications. 2025: John Wiley & Sons.

Ghai, I. and S. Ghai, Understanding antibiotic resistance via outer membrane permeability. Infection and drug resistance, 2018: p. 523-530.

Nikaido, H. and J.-M. Pagès, Broad-Specificity Efflux Pumps and Their Role in Multidrug Resistance of Gram-Negative Bacteria. FEMS microbiology reviews, 2012. 36(2): p. 340-363.

Garcia, Í.R., et al., Microbial resistance: The role of efflux pump superfamilies and their respective substrates. Life Sciences, 2022. 295(17): p. 120-391.

Vergalli, J., et al., Porins and small-molecule translocation across the outer membrane of Gram-negative bacteria. Nature Reviews Microbiology, 2020. 18(3): p. 164-176.

Gauba, A. and K.M. Rahman, Evaluation of antibiotic resistance mechanisms in gram-negative bacteria. Antibiotics, 2023. 12(11): p. 15-90.

Rajagopal, M. and S. Walker, Envelope structures of Gram-positive bacteria. Protein and sugar export and assembly in Gram-positive bacteria, 2017: p. 1-44.

Jubeh, B., Z. Breijyeh, and R. Karaman, Resistance of gram-positive bacteria to current antibacterial agents and overcoming approaches. Molecules, 2020. 25(12): p. 28-58.

Liu, X., et al., Simultaneous quantification of chrysophanol and physcion in rat plasma by ultra fast liquid chromatography–tandem mass spectrometry and application of the technique to comparative pharmacokinetic studies of Radix et Rhei Rhizoma extract alone and Dahuang fuzi decoction. Journal of Chromatography B, 2015. 980(6): p. 88-93.

Kiprotich, S., Isolation and structure determination of phytochemicals from *Senna didymobotrya* leaf extract used in cancer management. 2023, Makerere University.

Wang, Z.W., et al., Developmental Changes in the Composition of Five Anthraquinones from Rheum palmatum as Quantified by ^{1}H-NMR. Phytochemical Analysis, 2013. 24(4): p. 329-335.

Luyen, L.H., P.M. Quan, and N.P. Hung, Protein Tyrosine Phosphatase 1B Inhibitory Activities of Compounds Isolated from Polygonum cuspidatum. Vietnam Journal of Chemistry, 2019. 57(4): p. 496-499.

Adnan, M., et al., Physcion and physcion 8-O-β-D-glucopyranoside: Natural anthraquinones with potential anticancer activities. Current Drug Targets, 2021. 22(5): p. 488-504.

Liu, Y., et al., Physcion and physcion 8-O-β-glucopyranoside: A review of their pharmacology, toxicities and pharmacokinetics. Chemico-biological interactions, 2019. 310(1): p. 108-122.

Huang, D.-N., et al., The efficacy of natural bioactive compounds for the treatment of nasopharyngeal carcinoma. Mini Reviews in Medicinal Chemistry, 2021. 21(13): p. 1679-1691.

Dave, H. and L. Ledwani, A review on anthraquinones isolated from Cassia species and their applications. Indian Journal of Natural Products and Resources, 2012. 3(3): p. 291-319.

Feng, J., et al., Comparative analysis of the major constituents in three related polygonaceous medicinal plants using pressurized liquid extraction and HPLC-ESI/MS. Analytical Methods, 2016. 8(7): p. 1557-1564.

Škalamera, Đ., et al., Photochemical formation of anthracene quinone methide derivatives. The Journal of Organic Chemistry, 2017. 82(12): p. 6006-6021.

Korth, H.-G. and P. Mulder, Anthrone and related hydroxyarenes: Tautomerization and hydrogen bonding. The Journal of Organic Chemistry, 2013. 78(15): p. 7674-7682.

Yagi, S., et al., Chemical constituents and insecticidal activity of Senna italica Mill. from the Sudan. International letters of chemistry, Physics and Astronomy, 2013. 9(3): p. 146-151.

Fain, V.Y., B. Zaitsev, and M. Ryabov, Tautomerism of anthraquinones: V. 1, 5-Dihydroxy-9, 10-anthraquinone and its substituted derivatives. Russian Journal of Organic Chemistry, 2006. 42(11): p. 1662-1667. DOI: https://doi.org/https://doi.org/10.2174/138945012199920101315454 2.